Towards High-Resolution Imaging With Photonics-Based Time Division Multiplexing MIMO Radar

Fangzheng Zhang , *Senior Member, IEEE*, Guanqun Sun , Yuewen Zhou, Bindong Gao ,
and Shilong Pan , *Senior Member, IEEE*

(Invited Paper)

Abstract—A photonics-based time division multiplexing (TDM) multiple-input and multiple-output (MIMO) radar is proposed to realize high-resolution imaging. In this MIMO radar, multiple transmitters generate time-domain orthogonal linearly frequency modulated (LFM) signals based on microwave photonic frequency octupling and optical TDM technique, and multiple receivers implement dechirping of the multi-channel radar echoes based on microwave photonic frequency mixing. The microwave photonic techniques make the system capable to generate and process broadband radar signals, and the TDM yields a high spectral efficiency, which allows a large bandwidth in each transmitter and receiver. Meanwhile, the TDM-MIMO ensures complete orthogonality between different channels and enables good flexibility in arranging more transmit and receive channels. Therefore, the proposed photonics-based TDM-MIMO radar can achieve both high range resolution and high angular resolution. In the experiment, a photonics-based 4 × 8 TDM-MIMO radar is established which has an operation bandwidth of 8 GHz in each transmit channel. The range resolution and angular resolution are estimated to be 1.9 cm and 1.1°, respectively. A broadband back projection (BP) imaging algorithm with both frequency and time-delay dependent phase compensation is proposed, based on which high resolution imaging of single and complex targets is achieved.

Index Terms—Microwave photonics, radar, linearly frequency modulation (LFM), multiple-input and multiple-output (MIMO) time-division-multiplexing (TDM), back projection (BP) imaging.

I. INTRODUCTION

RADAR is one of the important means for humans to acquire the distance, azimuth, and velocity of a target

by transmitting a radio frequency signal and receiving the reflected echoes. In the development of radar technology, radar imaging is a milestone that greatly enhances the information acquisition capability and enables advanced radar functions such as high-accuracy target recognition [1]. As the detection environments become more and more complicated and variegated, future imaging radars should have a high resolution to acquire the fine information of targets, especially the small-size targets such as micro aerial vehicles. Currently, improving the range resolution of traditional radars is challenging because of the bandwidth limitation of electronic devices and subsystems [2]. Microwave photonics, which is an interdisciplinary subject combining the microwave and photonic technologies, provides new solutions for generation, transmission and processing of microwave signals [3]–[6]. Taking advantage of the high-frequency and broadband operation capability provided by photonic devices, microwave photonic technology is promising to significantly expand the radar frequency and bandwidth. Up to now, a number of photonics-based broadband radars have been proposed and successfully demonstrated [7]–[19]. The previous investigations have verified the feasibility as well as the advantages of photonics-based broadband radars, especially in achieving an ultra-high range resolution that reaches several millimeters [18], [19].

To achieve a high angular resolution and enable flexible beam scanning, combining the photonics-based broadband radar with array radar technology is an inevitable trend [20], [21]. For photonics-based phased array radars, as the operation bandwidth is enlarged, beam squint problem, i.e., the beam directions for different frequencies are divergent, becomes serious [22]. To address this problem, various optical true time delay (TTD) techniques have been intensively investigated [23]–[26]. Although an optically controlled phased array radar applying TTD technique can perform wideband beamforming, the system usually has a high complexity especially when the phased array is composed of a large number of elements. More importantly, the limited resolution of current optical TTD technique makes it difficult for beamforming in the high frequency range because the required time-delay step is very small, e.g., a TTD resolution of less than 0.1 ps is required for systems that are operated at

the 60-GHz frequency band. Recently, a new type of photonics-based phased array radar was proposed using photonic broadband dechirp processing in the receiver array [27]. This method is proved to be an effective solution for broadband beamforming by enabling flexible digital TTD compensation and multi-beam forming without complicated analog TTD networks. However, a large number of array elements are still required to achieve a high angular resolution. Multiple-input and multiple-output (MIMO) radar provides a good solution to construct a large size array with a small number of transmit and receive elements, because an $M \times N$ MIMO radar that has M transmitters and N receivers is equivalent to an array radar with MN array elements [28]. In a MIMO radar, the signals launched by the multiple transmitters should be orthogonal. Previously, photonics-based frequency-division-multiplexing (FDM)-MIMO radar has been demonstrated in which multiple transmitters launch radar signals in different spectral ranges [29]–[32]. The main drawback of this method is the low spectral efficiency, especially for the case when each channel has a broad bandwidth. The low spectral efficiency also limits the number of transmit channels, and thus restricting the size of the equivalent array. In addition to photonics-based FDM-MIMO radars, photonics-based code-division-multiplexing (CDM) MIMO architecture has also been applied to construct a fully coherent distributed radar network in [33]. Since extra phase coding models are required in multiple transmit channels, the system complexity is increased. What's more, the non-ideal orthogonality of CDM easily results in crosstalk between different channels.

In this paper, we propose a photonics-based broadband time-division-multiplexing (TDM)-MIMO radar and investigate its performance for high-resolution imaging. In the proposed photonics-based TDM-MIMO radar, the multiple transmitters generate multi-channel orthogonal linearly-frequency modulated (LFM) signals based on microwave photonic frequency octupling and optical time division multiplexing. In the multiple receivers, microwave photonic frequency mixing is applied to dechirp the multiple radar echoes corresponding to different transmit channels. Thanks to the microwave photonic signal generation and processing techniques, the radar transceivers can be operated in a large spectral range. Besides, the TDM mechanism allows a high spectral efficiency, permitting a large operation bandwidth in each transmit channel. Meanwhile, the TDM manner ensures complete orthogonality between different channels and good flexibility in arranging more channels. As a result, the photonics-based TDM-MIMO radar has both high range resolution and high angular resolution. In the experiment, a photonics-based 4×8 TDM-MIMO radar is built with a bandwidth of 8 GHz in each transmit channel. The measured range resolution and angular resolution are 1.9 cm and 1.1°, respectively. To implement radar imaging, a broadband back projection (BP) imaging algorithm is proposed in which both frequency and time-delay dependent phase compensation is conducted, instead of time-delay dependent phase compensation in narrowband BP imaging. With this method, high resolution imaging of both single and complex targets is demonstrated.

This paper is organized as follows. In Section II, the principle and experimental validation of a photonics-based monostatic
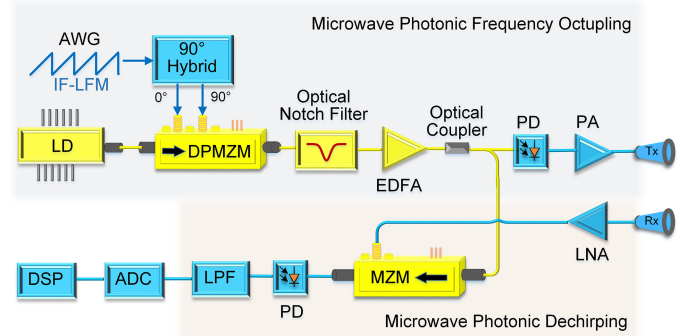

Fig. 1.   The structure of the photonics-based monostatic radar.

radar are introduced, which is the foundation to construct the TDM-MIMO radar. In Section III, the structure and principle of the photonics-based TDM-MIMO radar are presented, and design of the photonics-based 4×8 TDM-MIMO radar used in the experiment is discussed. Then, high-resolution imaging is demonstrated based on the photonics-based TDM-MIMO radar. Finally, conclusions are drawn in Section IV.

II. PHOTONICS-BASED MONOSTATIC RADAR

In this section, we introduce the photonics-based broadband monostatic radar, which is the basic element to construct the photonics-based TDM-MIMO radar. First, operation principle of the microwave photonic signal generation and processing in the radar transceiver is presented. Then, experimental results validating the feasibility and range resolution of the photonics-based monostatic radar are provided and discussed.

A. Principle of the Photonics-Based Monostatic Radar

Fig. 1 shows the structure of the photonics-based monostatic radar. In the transmitter, a broadband LFM signal is generated by microwave photonic frequency octupling. In the receiver, the radar echoes are dechirped based on microwave photonic frequency mixing. As shown in Fig. 1, the continuous wave (CW) light generated by a laser diode (LD) is modulated by a dual-parallel Mach-Zehnder modulator (DPMZM) that is driven by an intermediate frequency (IF)-LFM signal. The instantaneous frequency of the IF-LFM signal is

$$f_{\text{IF}-\text{LFM}}(t) = f_0 + kt(0 \leq t \leq T) \tag{1}$$

where f_0, k and T are the initial frequency, chirp rate, and pulse width, respectively. Before applied to drive the DPMZM, the IF-LFM signal passes through an electrical 90° hybrid to produce two signals having a 90° phase difference between each other. The DPMZM is composed of two parallelly installed Mach-Zehnder modulators (MZM-a and MZM-b), as shown in Fig. 2. Both of the two MZMs are biased at the maximum transmission points to suppress the odd-order modulation sidebands [34]. By properly setting the amplitudes of the IF-LFM signals, the frequency components of the optical carrier, the $\pm 2^{\text{nd}}$-order modulation sidebands and the $\pm 4^{\text{th}}$-order modulation sidebands dominate the output signals from MZM-a and MZM-b. By
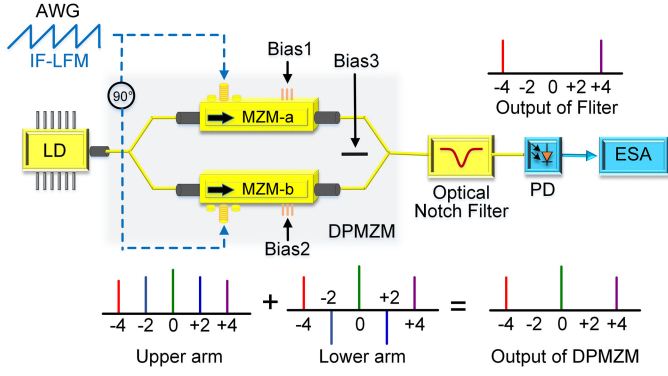
Fig. 2. Principle of the microwave photonic frequency octupling.

setting the third bias voltage of the DPMZM to let the two arms in phase, the output signal from the DPMZM only contains the optical carrier and $\pm 4^{th}$-order modulation sidebands. Following the DPMZM, an optical notch filter is applied to block the optical carrier, outputting an optical signal composed by only the $\pm 4^{th}$-order modulation sidebands, which can be expressed as

$$e_{\text{filter}}(t) \propto J_4(\alpha) \exp[j2\pi(f_c + 4f_0 + 2kt)t]$$
$$+ J_4(\alpha) \exp[j2\pi(f_c - 4f_0 - 2kt)t] \quad (2)$$

where f_c is the frequency of the CW light, α is the modulation index, and $J_4(\cdot)$ is the 4th-order Bessel function of the first kind. The output signal is amplified by an erbium-doped fiber amplifier (EDFA) before it is split into two branches using an optical coupler. The signal in the upper branch is fed to a photodetector (PD) to perform optical-to-electrical conversion, generating the following electrical signal

$$i(t) \propto J_4^2(\alpha) \cos[2\pi(8f_0 + 4kt)t] \quad (3)$$

The instantaneous frequency of the generated signal in Eq. (3) is $8f_0 + 8kt$. Thus, a frequency-octupled LFM signal is generated that has a bandwidth of $8kT$. This signal is properly amplified by a power amplifier (PA) and launched to the detection area through a transmit antenna (Tx).

The radar echo collected by the receive antenna (Rx) is amplified by a low noise amplifier (LNA). The obtained signal is fed to another MZM to modulate the reference optical signal from the lower branch of the optical coupler. The optical signal after MZM is given as

$$e_{\text{MZM}}(t) \propto J_4(\alpha) \exp[j2\pi(f_c + 4f_0 + 2kt)t]$$
$$+ J_4(\alpha) \exp[j2\pi(f_c - 4f_0 - 2kt)t]$$
$$+ J_4(\alpha)J_1(\beta) \exp[j2\pi(f_c + 4f_0 + 2kt - 8k\tau)t]$$
$$+ J_4(\alpha)J_1(\beta) \exp[j2\pi(f_c - 4f_0 - 2kt + 8k\tau)t]$$
$$+ \cdots \quad (4)$$

where β is the modulation index at the MZM and τ is the delay time of the radar echo referenced to the transmitted LFM signal. In obtaining Eq. (4), only the $\pm 1^{st}$-order modulation

sidebands are considered. The optical signal from the MZM is sent to another PD where photonic frequency mixing occurs and dechirping of the radar echo is conducted [10]. Then, the dechirped signal is selected by a low pass filter (LPF), which is given as

$$S(t) \propto \cos[2\pi(8k\tau)t + \varphi_0] \quad (5)$$

in which φ_0 is a fixed phase term. The dechirped signal is digitized by an analog-to-digital converter (ADC) and the obtained digital signal is sent to a digital signal processing (DSP) unit. By performing fast Fourier transformation (FFT) to the sampled signal, the range profile along the radar line of sight can be obtained as [27]

$$R(r) = \{F[S(t)]\}_{f=2kr/c} \quad (6)$$

where r is the distance between radar and target, c is the speed of light and $F(\cdot)$ denotes the FFT operation. The range resolution is determined by [13]

$$R_{res} = \frac{c}{2B} \quad (7)$$

where $B = 8kT$ is radar bandwidth.

B. Experimental Validation

Based on the previous principle, a photonics-based monostatic radar having a bandwidth of 8 GHz is established. The CW light from an LD (TeraXion Inc.) has a wavelength of 1550.2 nm, and the DPMZM (Fujitsu FTM7962EP) used for frequency octupling has a 3-dB bandwidth of ~ 22 GHz. The IF-LFM signal generated by an arbitrary waveform generator (AWG: Keysight 8195A) has a bandwidth of 1 GHz (2.25-3.25 GHz) and a time duration of 10 μs. After the DPMZM, an optical programmable processer (Waveshaper 4000s Finisar Inc.) is used as the notch filter with a stopband of 10 GHz and a depth of 30 dB. The optical spectrum of the output signal is shown in Fig. 3(a), in which the $\pm 4^{th}$-order modulation sidebands are successfully generated with the optical carrier well suppressed by over 20 dB. After optical-to-electrical conversion at a PD (u2t XPDV2120RA; Bandwidth: 40 GHz), an LFM signal with a bandwidth of 8 GHz (18-26 GHz) is generated. The waveform of the obtained LFM signal is recorded by a real-time oscilloscope (Keysight DSO-X 93204A) with a sampling rate of 80 GSa/s, as shown in Fig. 3(b). By performing short-time Fourier transformation (STFT) to the sampled signal, the time-frequency diagram of the LFM signal is obtained, as shown in Fig. 3(c). As can be seen, a frequency-octupled LFM signal covering the frequency range of 18-26 GHz is successfully generated. Through further spectral analysis, the in-band signal-to-noise ratio (SNR) of the LFM signal is found to be 67 dB. The generated LFM signal is amplified by an amplifier (SHF 806E) before launched to the air through a K-band horn antenna (Bandwidth: 18-26.5 GHz; Gain: 15 dBi).

To investigate the performance of photonic dechriping, detection of two closely placed targets is implemented, with the experimental scene shown in Fig. 4(a). The targets are two corner reflectors (size: 1.3 cm × 1.3 cm × 1.3 cm) that are separated by 1.9 cm along the radar range direction. Here, the distance
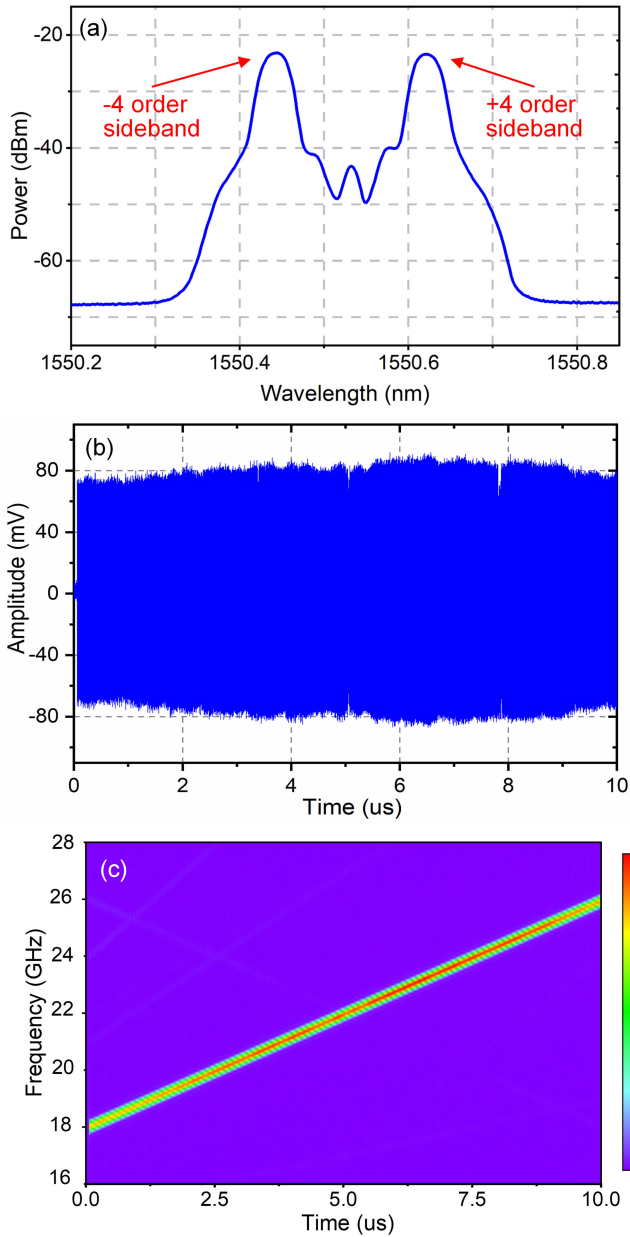
Fig. 3. (a) The optical spectrum after optical notch filter; (b) the time domain waveform of the generated frequency-octupled LFM signal and (c) the time-frequency diagram of the generated frequency-octupled LFM signal.

Fig. 4. (a) Picture of the dual-target detection scene in the experiment, (b) the sampled waveform of the dechirped siganls, and (c) the corresponding ragne profile.

between the two targets is chosen to validate the radar range resolution, of which the theoretical value is 1.875 cm. The radar echoes collected by a K-band receive antenna are amplified by another amplifier (SHF 806E) before used to drive an MZM (Fujitsu FTM7938; Bandwidth: ∼28 GHz). The output optical signal is sent to a PD (CONQUER Inc; Bandwidth: 10 GHz) to implement microwave photonic frequency mixing. An LPF with a bandwidth of 100 MHz is applied to select the dechirped signal, which is then sampled by an ADC with a sampling rate of 200 MSa/s. The waveform of the dechirped signal is shown in Fig. 4(b). Based on Eq. (6), the range profile is calculated and shown in Fig. 4(c). As shown in Fig. 4(c), two resolvable peaks corresponding to the two targets are observed at 1.16 m and 1.18
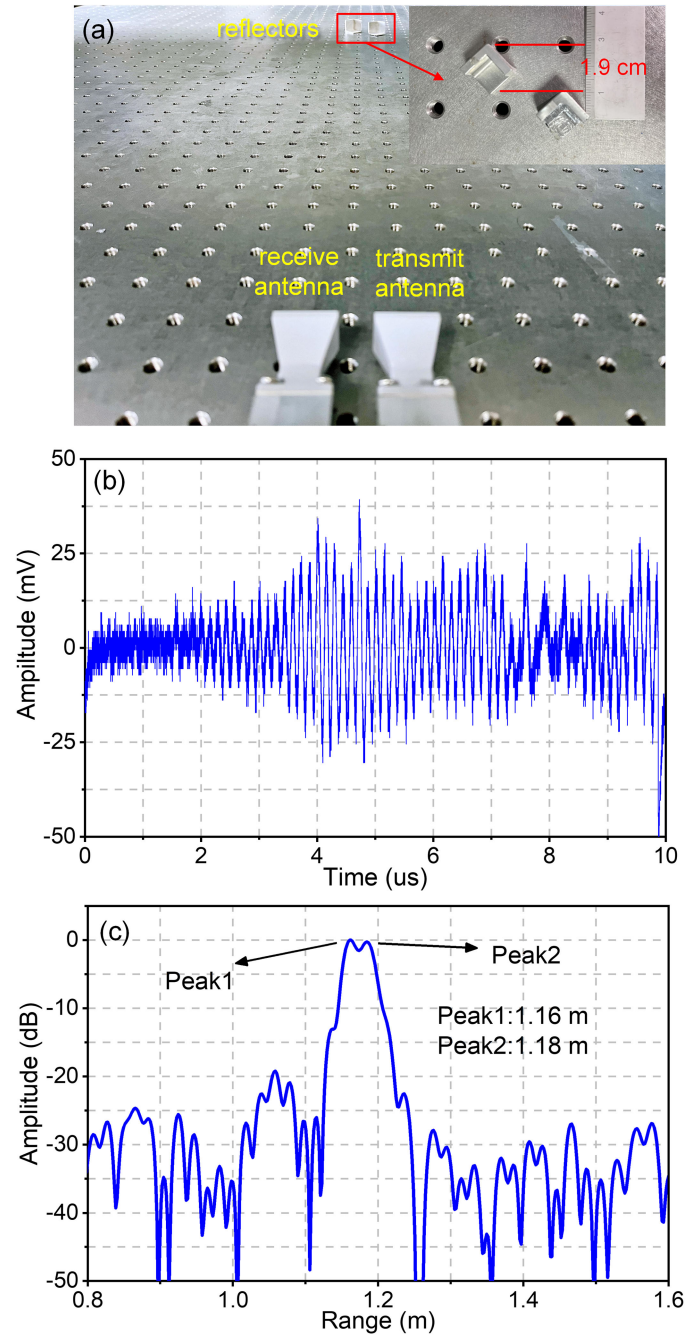
m, respectively. The measured spacing between the two targets is 2 cm, which is very close to the real distance. These results can soundly validate the photonic dechriping capability as well as the range resolution of the photonics-based monostatic radar.

III. PHOTONICS-BASED TDM-MIMO RADAR

In this section, we introduce the structure and principle of the photonics-based TDM-MIMO radar constructed based on the photonics-based monostatic radar. A photonics-based 4 × 8 TDM-MIMO radar with an operation bandwidth of 8 GHz is
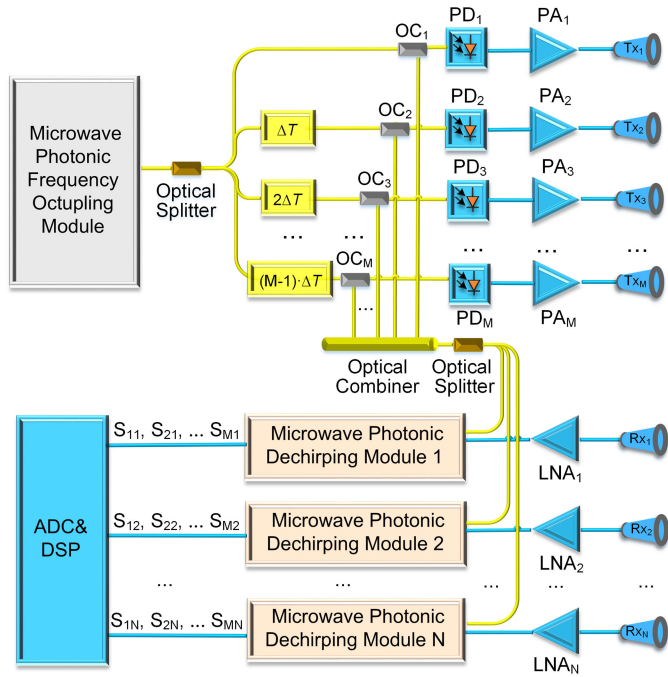
Fig. 5. Schematic diagram of the photonics-based TDM-MIMO radar.

Fig. 6. (a) Sequential relationship of the transmitted TDM signals, (b) illustration of the dechirping in Rx1.

experimentally established, based on which high-resolution BP imaging is demonstrated.

A. Principle of the Photonics-Based TDM-MIMO Radar

Fig. 5 shows the schematic diagram of a photonics-based $M \times N$ TDM-MIMO radar which contains M transmitters and N receivers. The microwave photonic frequency octupling module generates an optical frequency octupling modulation signal based on the principle in Section II. In this module, the pulsed IF-LFM signal has a pulse width of T_0 and a repetition rate of $f_{\rm rep}$. The obtained optical signal is split into M channels by an optical splitter. An optical time delay of ΔT is introduced to adjacent channels using multiple fiber delay lines, which completes the time-division multiplexing. Each delayed optical signal is divided into two branches by an optical coupler. The signals in the upper branches are sent to multiple PDs to generate M frequency octupled LFM signals that are mutually orthogonal in time domain. The generated LFM signals have the same pulse width and duty cycle as those of the IF-LFM signal, as shown in Fig. 6(a), in which the temporal period of each transmit channel is $T = 1/f_{\rm rep}$. These signals are amplified by multiple power amplifiers before launched to the detection area through M transmit antennas. At the same time, the multiple optical signals from the lower branches of the optical couplers are combined by an optical combiner and then split into N branches by an optical splitter. The signal in each branch is used as the optical reference signal for dechirp processing in the N receivers.

The radar echoes collected by each receive antenna are amplified before sent to the microwave photonic dechirping module together with the reference optical signal. The basic principle of dechirping is the same as the single channel dechiping introduced in Session II, except that the dechirping of radar echoes
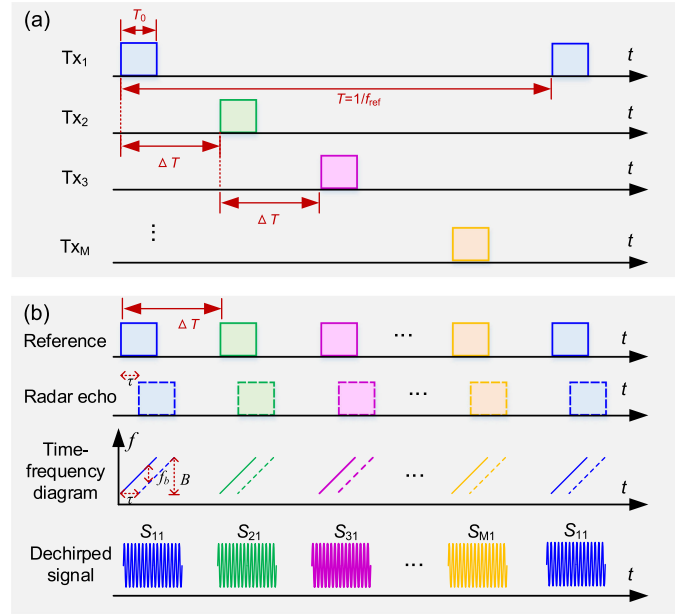
corresponding to different transmitters is implemented in a TDM manner. To show this clearly, the dechirping process in the first receiver (Rx1) is shown in Fig. 6(b), where the sequential relationships of the reference and echo are illustrated. After N-channel analog-to-digital conversions, the dechirped signals corresponding to multiple orthogonal transmit channels can be easily separated in time domain. This way, MN dechirped signals (S_{ij}) corresponding to the $i^{\rm th}$ transmitter and the $j^{\rm th}$ receiver ($i = 1, 2, 3 \ldots M; j = 1, 2, 3 \ldots N$) are obtained, based on which target detection and imaging can be implemented in the DSP unit.

To ensure that the radar echoes corresponding to the M transmit antennas can be separated without aliasing and well dechirped by the reference signal, the following equations should be satisfied

$$2T_0 < \Delta T \leq T/M$$
$$R_{\max} < T_0 c/2 \tag{9}$$

where $R_{\max}$ is the maximum detection range of the radar. According to Eq. (9), the parameters of the signal, including the duty cycle of each channel and the time delay between adjacent channels can be designed, and the maximum detection range of the radar can be estimated. In applications of specific occasions, other factors should be considered in addition to Eq. (9), e.g., the detection of a fast-moving target prefers a small ΔT and a large $f_{\rm rep}$.

An $M \times N$ MIMO array is equivalent to an array with one transmit antenna and MN receive antennas. In this paper, a linear array shown in Fig. 7 is adopted in which the spacing between adjacent receive antennas is d and the spacing between adjacent transmit antennas is Nd. According to the spatial convolution principle [35], the equivalent receiving array is a uniform linear array (ULA) that contains MN antennas with an element spacing
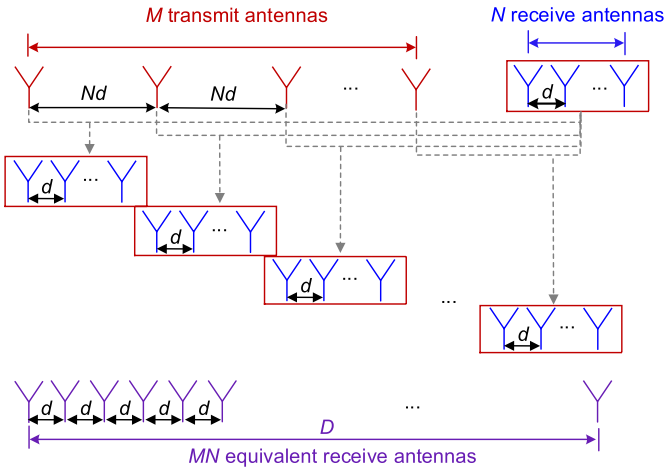
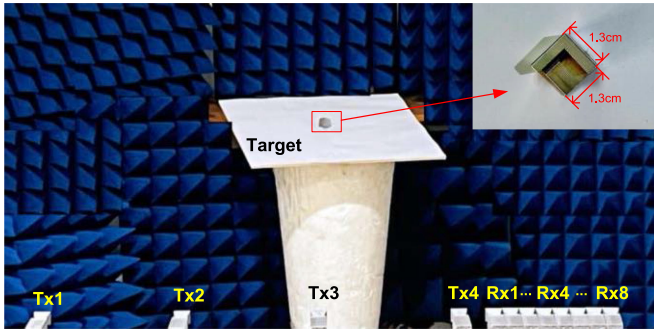Fig. 7.   Configuration of the photonics-based $M \times N$ TDM-MIMO radar array.

Fig. 8.   Picture of the MIMO radar array and a conner reflector as the target.

of d. For the photonics-based TDM-MIMO radar, the range resolution is still determined by Eq. (7), and the angular resolution is determined by [36]

$$\theta_{res} = \frac{\lambda_c}{\pi D} \cdot 180° \qquad (8)$$

where D is the size of the equivalent receiving array and λ_c is the central wavelength of the radar signal.

B. Experimental Parameters and Multi-Channel Dechirping

A photonics-based 4×8 TDM-MIMO radar is established in the experiment. The LFM signal generated by microwave photonic frequency ocpuling has a bandwidth of 8 GHz (18-26 GHz) and a pulse width of 10 μs. The repetition rate is 12.5 kHz and the pulse duty cycle is 12.5%. A time delay of 20 μs is introduced between adjacent transmit channels using optical delay lines. Four PDs are used to implement optical-to-electrical conversions, generating four time-division-multiplexed LFM signals. Due to the hardware constraints, the eight receive antennas use the same receiver to collect the radar echoes in a time-division manner, and the receiver has the same parameters as those demonstrated in Section II.

The antenna array used in the experiment is shown in Fig. 8. Limited by the size of the horn antennas, the spacing between adjacent receive antennas (d) is set to 2.42 cm, which is 1.78

times the central wavelength. The spacing between adjacent transmit antennas (Nd) is set to 19.36 cm. The 4×8 MIMO array is equivalent to a receiving ULA with 32 elements. The element spacing of the equivalent ULA is 2.42 cm and the total aperture size is 75.02 cm. The beam divergence angle of each antenna is over 60°, which ensure a large irradiation area in azimuth direction.

To show the multi-channel dechirping capability of the photonics-based TDM-MIMO radar, detection of a single corner reflector is demonstrated. The corner reflector is placed at a distance of about 1.6 m away from the MIMO array, as shown in Fig. 8. Based on the 32 dechirped signals, the range profiles can be calculated, among which the normalized range profiles corresponding to S_{11}, S_{21}, $S_{31,}$ and S_{41} are selected, as shown in Figs. 9(a)-(d), respectively. As shown in Fig. 9, a single peak corresponding to the position of the corner reflector is observed in all the four range profiles, verifying that dechirping and separation of the radar echoes of multiple channels are successfully conducted. The target distance measured by different channels is also shown in Fig. 9. It should be noted that, because of the different observation angles, the measured distances in Fig. 9 are slightly different.

C. Photonics-Based TDM-MIMO Radar Imaging

Thanks to the broad bandwidth and large equivalent aperture size, the photonics-based TDM-MIMO radar has the capability of imaging with both a high range resolution and a high angular resolution. However, as the range resolution is remarkably improved, the target distance measured by different channels would easily fall in different range resolution cells, i.e., the distance variation is larger than the radar range resolution, as indicated by the results in Fig. 9. This problem is similar with the range migration effect in synthetic aperture radar imaging, which causes de-focusing when using typical frequency-domain algorithms to construct the image [37]. To deal with this problem, we adopt the BP imaging method, which is a time-domain radar imaging method using the time-delay information to avoid the influence of range migration [38], [39].

The basic principle of BP imaging with the photonics-based TDM-MIMO radar is as follows. First, multi-channel data arrangement is carried out to let the MN dechirped signals be matched to the equivalent ULA. Then, MN range profiles are calculated according to Eq. (6), and all the range profiles are mapped to the desired imaging pixels through interpolation, obtaining MN coarse images [40]. At last, all the coarse images are accumulated coherently to get a 2D image. For narrow-band BP imaging, a time-delay related phase term should be compensated to realize coherent accumulation [41]. The amplitude of the pixel at the coordinate of (x_i, y_j) is obtained by

$$A(x_i, y_j) = \sum_{l=1}^{M \times N} R_l(t_{ij}) \exp(j2\pi f_{co} t_{ij}) \qquad (10)$$

where t_{ij} is the round-trip time delay between the lth equivalent array element ($l = 1, 2, \ldots, MN$) and the pixel at (x_i, y_j), and f_{co} is the center frequency of the radar signal. However, for the photonics-based TDM-MIMO radar that has a very broad
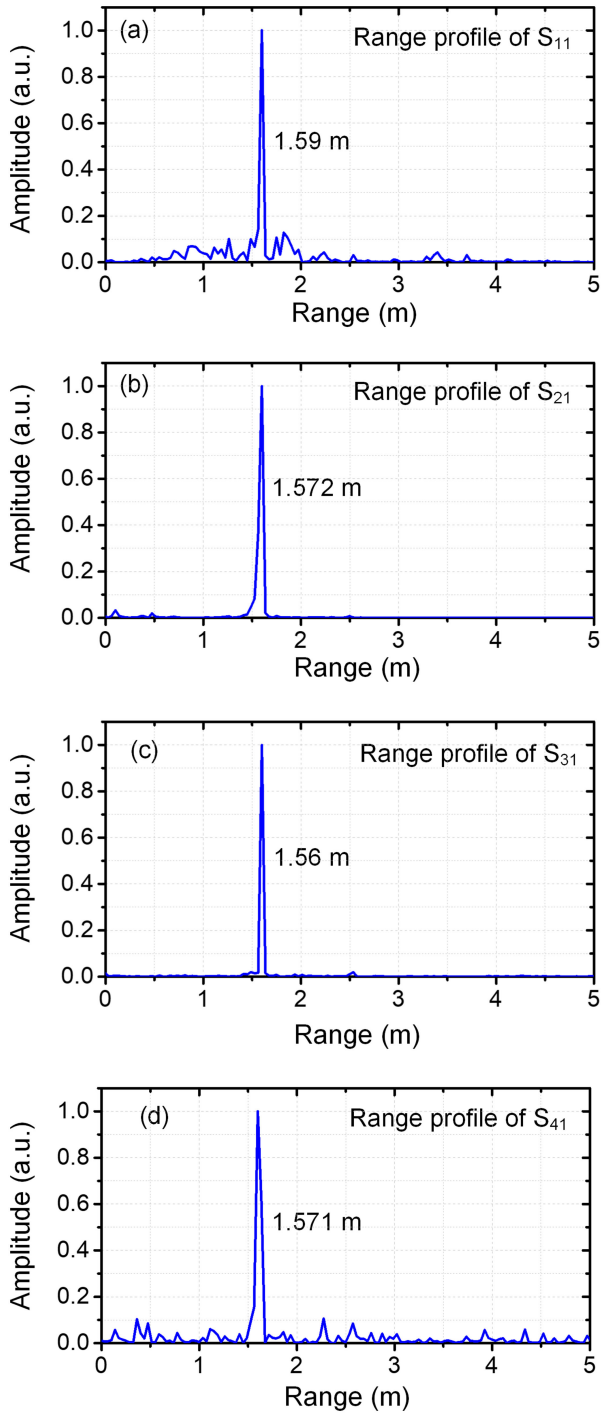
Fig. 9. (a) The range profile of S_{11}, (b) the range profile of S_{21}, (c) the range profile of S_{31}, and (d) the range profile of S_{41}.

bandwidth, a given time delay corresponds to different phases for different frequencies. Thus, both frequency and time-delay dependent phase compensation is required in the coherent accumulation process. To this end, the center position of the desired imaging area is selected as the reference point, and the round-trip time delay between the lth equivalent array element and the reference point is denoted by t_{ref}. In addition to the phase term in Eq. (10), an extra phase of $\Delta\varphi_{ij}$ should also be compensated,
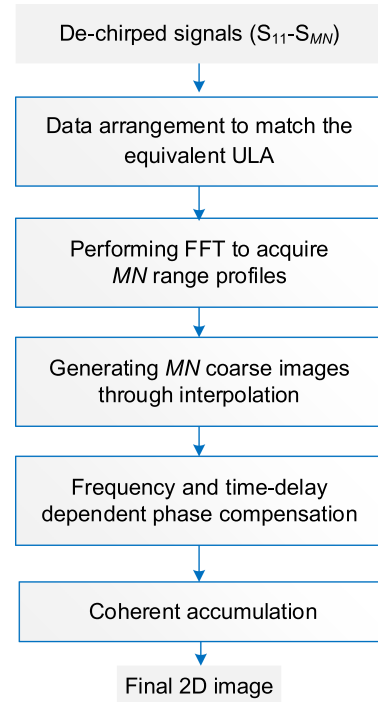

Fig. 10. Signal processing flow of the photonics-based broadband TDM-MIMO radar imaging.

and $\Delta\varphi_{ij}$ is determined by

$$\Delta\varphi_{ij} = 2\pi \cdot \Delta\tau_{ij} k' \cdot t_{ij} \tag{11}$$

in which $\Delta\tau_{ij} = t_{ij} - t_{\text{ref}}$, and k' is the chirp rate of the radar signal ($k' = 8k$). In this case, the amplitude of the pixel at (x_i, y_j) is obtained by

$$A_{\text{co}}(x_i, y_j) = \sum_{l=1}^{M \times N} R_l(t_{ij}) \exp(j2\pi f_{co} t_{ij}) \exp(j\Delta\varphi_{ij}) \tag{12}$$

The detailed processing flow of the proposed broadband BP imaging is shown in Fig. 10.

To investigate the imaging performance of the photonics-based 4×8 TDM-MIMO radar, the imaging of a single corner reflector shown in Fig. 8 is performed. As a comparison, we also construct the image obtained by a 1×8 array radar, aiming to show the influence of the array size on the imaging results. In the experiment, the 1×8 array radar is composed by Tx3 and all the eight receivers, of which the total receiving aperture size is 16.94 cm. When constructing the images, the proposed broadband BP imaging shown in Fig. 10 is applied. To get clean images without interference from the environment, background removal is implemented by subtracting the image without the target. The imaging results obtained by the 1×8 array radar and the 4×8 MIMO radar are shown in Fig. 11(a) and (b), respectively. It should be noted that, since the element spacing of the equivalent array is larger than half of the central wavelength, the grating lobe effect leads to the appearance of multiple image spots in different azimuths. Here, only the image spot corresponding to the actual azimuth is shown and investigated. In each of the two images shown in Fig. 11, a well-focused bright spot at the target
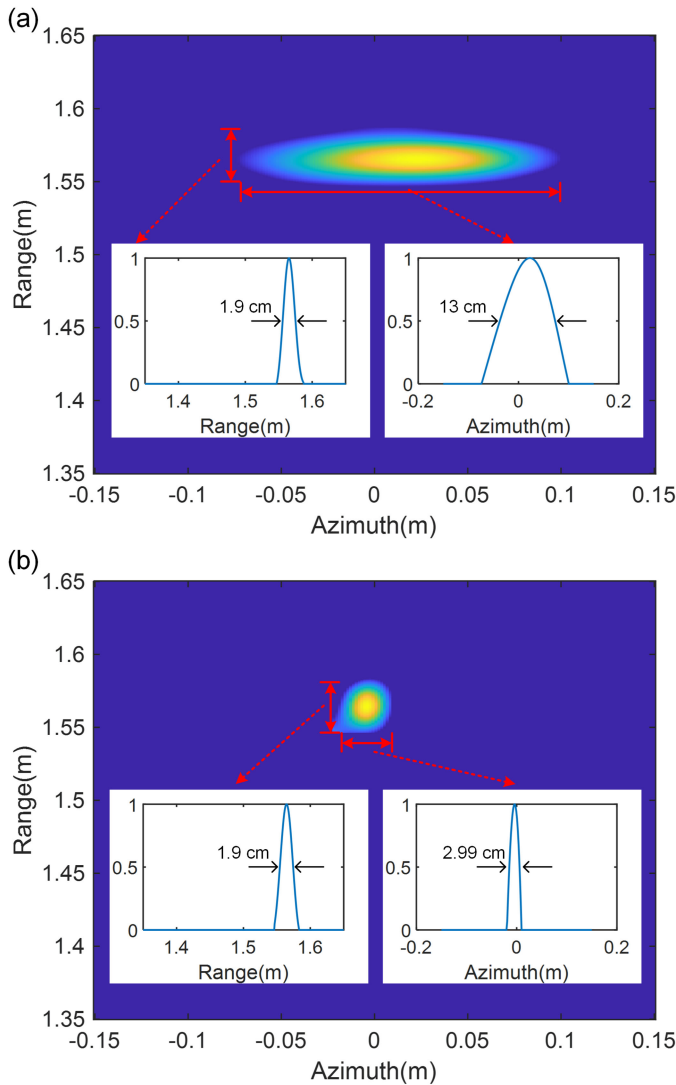
Fig. 11.   (a) The image obtained by the 1 × 8 array radar and (b) the image obtained by the 4 × 8 MIMO radar.

Fig. 12.   (a) The complex target with a "W" shape, (b) the image obtained by the 1 × 8 array radar and (c) the image obtained by the 4 × 8 MIMO radar.

position is observed, indicating the radar imaging is successfully implemented. By analyzing the peak widths of the range and azimuth profiles of the two bright image spots, the approximate range resolution and angular resolution of the two array radars can be acquired. Specifically, the range resolutions for the two conditions are both 1.9 cm. The angular resolution is calculated to be 4.8° and 1.1°, for the 1 × 8 array radar and the 4 × 8 MIMO radar, respectively. According to Eq. (8), the theoretical angular resolution of the two radars is 4.61° and 1.04°, respectively, both of which are close to the measured values. By comparing the images in Figs. 11(a) and (b), the capability of the MIMO radar in achieving a much higher angular resolution can be confirmed.

To further evaluate the radar imaging performance, a complex target is tested, which contains fifteen corner reflectors composing a "W" shape (size of each reflector: 2 cm × 2 cm × 2 cm), as shown in Fig. 12(a). Fig. 12(b) shows the constructed image with the 1 × 8 array radar. As can be seen, due to the relatively low angular resolution, the multiple reflectors

are overlapped and cannot be distinguished in the final image. When the 4 × 8 MIMO radar is applied, the obtained image is shown in Fig. 12(c). Thanks to the high resolutions in both the range and azimuth directions, the corner reflectors can be easily distinguished in the image constructed by the photonics-based 4 × 8 TDM-MIMO radar, and the shape of "W" can be clearly observed. Therefore, the complex target imaging result is a solid

proof showing the high-resolution imaging capability of the photonics-based TDM-MIMO radar.

IV. CONCLUSION

In conclusion, we have proposed a photonics-based TDM-MIMO radar and demonstrated its application in high-resolution imaging. The proposed radar uses microwave photonic frequency octupling together with TDM technique to generate broadband orthogonal LFM signals in the transmitters and uses microwave photonic frequency mixing for dechirping the multi-channel radar echoes. Compared with the previously reported photonics-based MIMO radar applying FDM and CDM mechanisms, the proposed photonics-based TDM-MIMO radar has a high spectral efficiency and a good orthogonality between different channels. This property makes the radar have a large operation bandwidth to achieve a high range resolution, and also enables a large number of channels or a large equivalent aperture size to achieve a high angular resolution. A photonics-based 4 × 8 MIMO radar with a bandwidth of 8 GHz in each channel is established, of which the range resolution and angular resolution are estimated to be 1.9 cm and is 1.1°, respectively. A BP imaging algorithm is proposed considering both frequency and time-delay dependent phase compensation, instead of time-delay dependent phase compensation in narrowband BP imaging. Based on the established MIMO radar and the proposed BP imaging method, imaging of both single and complex targets is demonstrated, through which the high resolution capability is verified.

REFERENCES

[1] D. A. Ausherman, A. Kozma, J. L. Walker, H. M. Jones, and E. C. Poggio, "Developments in radar imaging," *IEEE Trans. Aerosp. Electron. Syst.*, vol. AES-20, no. 4, pp. 363–400, Jul. 1984.

[2] P. Ghelfi *et al.*, "Photonics in radar systems: RF integration for State-of-the-Art functionality," *IEEE Microw. Mag.*, vol. 16, no. 8, pp. 74–83, Sep. 2015.

[3] A. Seeds and K. Williams, "Microwave photonics," *J. Lightw. Technol.*, vol. 24, no. 12, pp. 4628–4641, Dec. 2006.

[4] J. Capmany and D. Novak, "Microwave photonics combines two worlds," *Nature Photon.*, vol. 1, no. 6, pp. 319–330, Jun. 2007.

[5] J. Yao, "Microwave photonics," *J. Lightw. Technol.*, vol. 27, no. 3, pp. 314–335, Feb. 2009.

[6] S. Pan and Y. Zhang, "Microwave photonic radars," *J. Lightw. Technol.*, vol. 38, no. 19, pp. 5450–5484, Oct. 2020.

[7] D. Grodensky, D. Kravitz, and A. Zadok, "Ultra-wideband microwave-photonic noise radar based on optical waveform generation," *IEEE Photon. Technol. Lett.*, vol. 24, no. 10, pp. 839–841, May 2012.

[8] P. Ghelfi *et al.*, "A fully photonics-based coherent radar system," *Nature*, vol. 507, no. 7492, pp. 341–345, Mar. 2014.

[9] W. Zou, et al., "All optical central-frequency-programmable and bandwidth tailorable radar," *Sci. Rep.*, vol. 6, Jan. 2016, Art. no. 19786.

[10] F. Zhang *et al.*, "Photonics-based broadband radar for high-resolution and real-time inverse synthetic aperture imaging," *Opt. Exp.*, 25, no. 14, pp. 16274–16281, Jul. 2017.

[11] S. Peng *et al.*, "High-resolution W-band ISAR imaging system utilizing a logic-operation-based photonic digital-to-analog converter," *Opt. Exp.*, vol.ol. 26, no. 2, pp. 1978–1987, Jan. 2018.

[12] R. Li *et al.*, "Demonstration of a microwave photonic synthetic aperture radar based on photonic-assisted signal generation and stretch processing," *Opt. Exp.*, vol. 25, no. 13, pp. 14334–14340, Jun. 2017.

[13] F. Zhang, Q. Guo, and S. Pan, "Photonics-based real-time ultra-high-range-resolution radar with broadband signal generation and processing," *Sci. Rep.*, vol. 7, Oct. 2017, Art. no. 13848.

[14] Y. Tong *et al.*, "Photonics-based coherent wideband linear frequency modulation pulse signal generation," *Opt. Lett.*, vol. 43, no. 5, pp. 1023–1026, Mar. 2018.

[15] X. Ye, F. Zhang, Y. Yang, and S. Pan, "Photonics-based radar with balanced I/Q de-chirping for interference-suppressed high-resolution detection and imaging," *Photon. Res.*, vol. 27, no. 3, pp. 265–272, Mar. 2019.

[16] Y. Bae, J. Shin, S. G. Lee, and H. Kim, "Field experiment of photonic radar for low-RCS target detection and high-resolution image acquisition," *IEEE Access*, vol. 9, pp. 63559–63566, Apr. 2021.

[17] S. S. S. Panda, T. Panigrahi, S. R. Parne, S. L. Sabat, and L. R. Cenkeramaddi, "Recent advances and future directions of microwave photonic radars: A review," *IEEE Sens. J.*, vol. 21, no. 19, pp. 21144–21158, Oct. 2021.

[18] G. Sun, F. Zhang, and S. Pan, "Millimeter-level resolution through-the-wall radar imaging enabled by an optically injected semiconductor laser," *Opt. Lett.*, vol. 46, no. 12, pp. 5659–5662, Nov. 2021.

[19] X. Zhu, G. Sun, and F. Zhang, "Photonics-based multiband radar fusion with millimeter-level range resolution," in *Proc. Opt. Fiber Commun. Conf.*, 2022, Art. no. Th3G.2.

[20] S. Pan, X. Ye, Y. Zhang, and F. Zhang, "Microwave photonic array radars," *IEEE J. Microw.*, vol. 1, no. 1, pp. 176–190, Jan. 2021.

[21] J. Dong, F. Zhang, Z. Jiao, Q. Sun, and W. Li, "Microwave photonic radar with a fiber-distributed antenna array for three-dimensional imaging," *Opt. Exp.*, vol. 28, no. 13, pp. 19113–19125, Jun. 2020.

[22] H. Schrank, "Beam squint in parabolic reflector antennas with circularly polarized feeds," *IEEE Antennas Propag. Mag.*, vol. 32, no. 1, pp. 31–34, Feb. 1990.

[23] J. Corral, J. Marti, J. Fuster, and R. Laming, "True time-delay scheme for feeding optically controlled phased-array antennas using chirped-fiber gratings," *IEEE Photon. Technol. Lett.*, vol. 9, no. 11, pp. 1529–1531, Nov. 1997.

[24] D. Dolfi, F. Michel-Gabriel, S. Bann, and J. Huignard, "Two-dimensional optical architecture for time-delay beam forming in a phased-array antenna," *Opt. Lett.*, vol. 16, no. 4, pp. 255–257, Feb. 1991.

[25] X. Ye, F. Zhang, and S. Pan, "Compact optical true time delay beamformer for a 2D phased array antenna using tunable dispersive elements," *Opt. Lett.*, vol. 41, no. 17, pp. 3956–3959, Sep. 2016.

[26] O. Raz, S. Barzilay, R. Rotman, and M. Tur, "Submicrosecond scan-angle switching photonic beamformer with flat RF response in the c and x bands," *J. Lightw. Technol.*, vol. 26, no. 15, pp. 2774–2781, Aug. 2008.

[27] B. Gao, F. Zhang, E. Zhao, D. Zhang, and S. Pan, "High-resolution phased array radar imaging by photonics-based broadband digital beamforming," *Opt. Exp.*, vol. 27, no. 9, pp. 13194–13203, Apr. 2019.

[28] I. Bekkerman and J. Tabrikian, "Target detection and localization using MIMO radars and sonars," *IEEE Trans. Signal Process.*, vol. 54, no. 10, pp. 3873–3883, Oct. 2006.

[29] S. Maresca *et al.*, "Coherent dual-band 2 × 4 MIMO radar experiment exploiting photonics," in *Proc. 33rd Gen. Assem. Sci. Symp. Int. Union Radio Sci.*, Rome, Italy, 2020, pp. 1–4.

[30] G. Serafino *et al.*, "A photonics-assisted multi-band MIMO radar network for the port of the future," *IEEE J. Sel. Top. Quantum Electron.*, vol. 27, no. 6, Nov./Dec. 2021, Art. no. 6000413.

[31] F. Zhang, B. Gao, and S. Pan, "Photonics-based MIMO radar with high-resolution and fast detection capability," *Opt. Exp.*, vol. 26, no. 13, pp. 17529–17540, Jun. 2018.

[32] B. Gao, F. Zhang, G. Sun, Y. Xiang, and S. Pan, "Microwave photonic MIMO radar for high-resolution imaging," *J. Lightw. Technol.*, vol. 39, no. 24, pp. 7726–7733, Dec. 2021.

[33] X. Xiao *et al.*, "Photonics-based wideband distributed coherent aperture radar system," *Opt. Exp.*, vol. 26, no. 26, pp. 33783–33796, Dec. 2018.

[34] F. Zhang, X. Ge, and S. Pan, "Triangular pulse generation using a dual-parallel Mach-Zehnder modulator driven by a single-frequency RF signal," *Opt. Lett.*, vol. 38, no. 22, pp. 27017–27022, Nov. 2013.

[35] Y. Su, Y. Zhu, W. Yu, H. Xu, and W. Lei, "Multi-channel radar array design method and algorithm," *Sci. China Inf. Sci.,* vol. 53, no. 7, pp. 1470–1480, Jul. 2010.

[36] C. Balanis, *Antenna Theory: Analysis and Design*, 4th ed. New York, NJ, USA: Wiley, 2016.

[37] X. Zhuge and A. G. Yarovoy, "Three-dimensional near-field MIMO array imaging using range migration techniques," *IEEE Trans. Image Process.,* vol. 21, no. 6, pp. 3026–3033, Jun. 2012.

[38] G. Sun, et al., "Photonics-based 3D radar imaging with CNN-assisted fast and noise-resistant image construction," *Opt. Exp.,* vol. 29, no. 13, pp. 19352–19361, Jun. 2021.

[39] Y. Cho, H. Jung, C. Cheon, and Y. Chung, "Adaptive back-projection algorithm based on climb method for microwave imaging," *IEEE Trans. Magn.*, vol. 52, no. 3, pp. 1–4, Mar. 2016.

[40] G. Sun and F. Zhang, "Convolutional neural network (CNN)-based fast back projection imaging with noise-resistant capability," *IEEE Access*, vol. 8, pp. 117080–117085, Jul. 2020.

[41] L. Ulander, H. Hellsten, and G. Stenstrom, "Synthetic-aperture radar processing using fast factorized back-projection," *IEEE Trans. Aerosp. Electron. Syst.,* vol. 39, no. 3, pp. 760–776, Jul. 2003.

Fangzheng Zhang (Senior Member, IEEE) received the B.S. degree from the Huazhong University of Science and Technology, Wuhan, China, in 2008, and the Ph.D. degree from the Beijing University of Posts and Telecommunications, Beijing, China, in 2013. He is currently a Full Professor with the College of Electronic and Information Engineering, Nanjing University of Aeronautics and Astronautics, Nanjing, China. His main research interests include microwave photonics, radar imaging, and machine learning.

Guanqun Sun received the B.S. degree from Northwestern Polytechnical University, Xi'an, China, in 2018, and the M.S. degree in 2021 from the Nanjing University of Aeronautics and Astronautics, Nanjing, China, where he is currently working toward the Ph.D. degree with the Key Laboratory of Radar Imaging and Microwave Photonics, Ministry of Education. His research focuses on photonics-based radars for high resolution imaging.

Yuewen Zhou received the B.S. degree in information engineering in 2019 from the Nanjing University of Aeronautics and Astronautics, Nanjing, China, where she is currently working toward the Ph.D degree with the Key Laboratory of Radar Imaging and Microwave Photonics, Ministry of Education. Her research interests include microwave photonic radar signal processing.

Bindong Gao received the B.S. and Ph.D. degrees in information engineering from the Nanjing University of Aeronautics and Astronautics, Nanjing, China, in 2015 and 2021, respectively. His research focuses on microwave photonics, which include optical generation of microwave signals and design of microwave photonic array radar system.

Shilong Pan (Senior Member, IEEE) is currently a Professor with the Nanjing University of Aeronautics and Astronautics, Nanjing, China. He has authored or coauthored more than 300 papers in peer-reviewed journals. His research focused on microwave photonics, which include optical generation and processing of microwave signals, analog photonic links, photonic microwave measurement, and integrated microwave photonics. Prof. Pan is currently an Associate Editor of the *Electronics Letters*, the Topical Editor of the PhotoniX, the Deputy Editor of *Chinese Optics Letters,* and the Vice Chair of IEEE MTT-22 Microwave Photonics. He is a Steering Committee Member of the IEEE/OSA JOURNAL OF LIGHTWAVE TECHNOLOGY. He was also the Chair of a number of international conferences, symposia, and workshops, including the TPC Chair of IEEE ICOCN 2015, TPC Co-Chair of IEEE MWP2017, and General Co-Chair of IEEE MWP2021. Prof. Pan is a Fellow of OSA, SPIE, and IET. He was selected as an IEEE Photonics Society Distinguished Lecturer in 2019 and was the recipient of IEEE MTT-S Outstanding Young Engineer Award in 2021.